JACS
JOURNAL OF THE AMERICAN CHEMICAL SOCIETY
Article
pubs.acs.org/JACS

Synthesis of Two-Dimensional Analogues of Copolymers by Site-to-Site Transmetalation of Organometallic Monolayer Sheets

Zhikun Zheng,*[,†] Lothar Opilik,[‡] Florian Schiffmann,[§] Wei Liu,[∥] Giacomo Bergamini,[⊥] Paola Ceroni,[⊥] Lay-Theng Lee,[#] Andri Schütz,[†] Junji Sakamoto,[†] Renato Zenobi,[‡] Joost VandeVondele,[§] and A. Dieter Schlüter*[,†]

[†]Laboratory of Polymer Chemistry, Institute of Polymers, Department of Materials, ETH Zürich, Vladimir-Prelog-Weg 5, CH-8093 Zürich, Switzerland

[‡]Laboratory of Organic Chemistry, Department of Chemistry and Applied Biosciences, ETH Zürich, Vladimir-Prelog-Weg 3, CH-8093 Zürich, Switzerland

[§]Nanoscale Simulations, Department of Materials, ETH Zürich, Wolfgang-Pauli-Strasse 27, CH-8093 Zürich, Switzerland

[∥]Physical Chemistry and Electrochemistry, Technical University Dresden, Bergstrasse 66b, 01062 Dresden, Germany

[⊥]Department of Chemistry "G. Ciamician", University of Bologna, Via Selmi 2, 40126 Bologna, Italy

[#]Laboratoire Léon Brillouin, CEA-Saclay, 91191 Gif-sur-Yvette Cedex, France

Supporting Information

ABSTRACT: Monolayer sheets have gained attention due to the unique properties derived from their two-dimensional structure. One of the key challenges in sheet modification/synthesis is to exchange integral parts while keeping them intact. We describe site-to-site transmetalation of Zn^{2+} in the netpoints of cm^2-sized, metal−organic sheets by Fe^{2+}, Co^{2+}, and Pb^{2+}. This novel transformation was done both randomly and at predetermined patterns defined by photolithography to create monolayer sheets composed of different netpoints. All transmetalated sheets are mechanically strong enough to be spanned over 20 × 20 μm^2 sized holes. Density functional theory calculations provide both a model for the molecular structure of an Fe^{2+}-based sheet and first insights into how transmetalation proceeds. Such transmetalated sheets with random and patterned netpoints can be considered as two-dimensional analogues of linear copolymers. Their nanoscale synthesis presents an advance in monolayer/polymer chemistry with applications in fields such as surface coating, molecular electronics, device fabrication, imaging, and sensing.

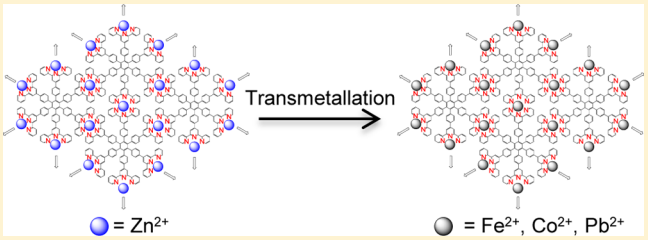

1. INTRODUCTION

Monolayer sheets have gained intense attention due to the unique physical and chemical properties derived from their two-dimensional structure, which sets them apart from bulk matter as well as from, for example, nanotubes and nanoparticles.[1−4] Examples include single layers of graphene,[1,2] hexagonal boron nitride,[1] and layered metal chalcogenides.[5] If not provided by nature, these monolayer sheets are typically obtained from thermolytic and other high-energy procedures. Noteworthy examples are the graphene synthesis from organic precursors at high temperature,[6] the generation of structured sheets, such as those composed of graphene and boron nitride parts,[7−10] and the nanosheets obtained from electron-beam-induced cross-linking of self-assembled monolayers.[11] The harsh experimental conditions needed for the synthesis of the above-mentioned sheets preclude molecular design on demand, and vigorous efforts have therefore been made into rational sheet synthesis under mild (organic) conditions. This has led to a number of interesting developments[12−22] which are based either on exfoliation of laminar crystals whose individual layers of specially designed monomers had priorly been polymerized or on surface-assisted synthesis in which monomers spread in monolayers at the air/water interface were connected with one another. The objects created include two-dimensional polymers (2DPs)[12−15] that are free-standing polymers with topologically planar repeat units[13] and a series of both covalent and metal−organic sheets for which structure analysis has not yet reached the point to show whether or not they have the internal periodicity to qualify as 2DPs.[16−18] Additionally, self-assembled systems were reported.[23,24]

Important representatives for the metal−organic sheets, **S1**(Met^{2+}) and **S2**(Met^{2+}), are shown in Figure 1 together with the terpyridine (tpy)-based monomers **1** and **2**, from which they were created by transition metal ion connectors, Met^{2+}, via $[Met(tpy)_2]^{2+}$ complexes as netpoints. Not all tpy units are engaged in netpoints, though, and first XPS-based conversion data suggest a strong dependence on the nature of

Received: February 21, 2014
Published: March 27, 2014

   dx.doi.org/10.1021/ja501849y | J. Am. Chem. Soc. 2014, 136, 6103−6110

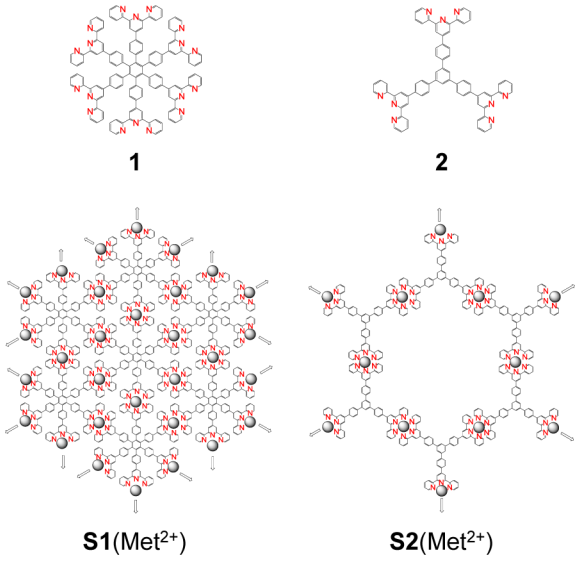

Figure 1. Idealized chemical structures of sheets **S1**(Met^{2+}) and **S2**(Met^{2}). Compounds **1** and **2** are the hexa- and trifunctional terpyridine (tpy)-based monomers and Met^{2+} for the transition metal ion used as connector resulting in $[Met(tpy)_2]^{2+}$ netpoints. Note that the two tpy engaged in each netpoint are likely to stand orthogonal to one another.

the metal ion used. For Zn^{2+} and Fe^{2+}, typical values are 55–74% for **S1**(Zn^{2+}), 60–79% for **S2**(Zn^{2+}), 64% for **S1**(Fe^{2+}), and 81% for **S2**(Fe^{2+}).[17]

Properties of existing sheets can, in principle, be modified by exchanging their constituents, very much like can be done for some linear polymers by exploiting equilibria between polymer and (new and different) monomer or in metal alloys by melting in another metallic component. This obviously requires the sheets to be held together by constituents between which there are active equilibrium processes that can be interfered with and that there is a molecular mechanism through which the exchange can be brought about. Metal–organic sheets, in principle, are equilibrium structures and therefore potential candidates for such attractive strategies. For crystalline metal–organic frameworks (MOFs), attempts have been reported in which mostly the metal ion connectors were exchanged by transmetalation.[22] This so far concerned metal ions complexed to carboxylates and other monodentate ligands/anions.[25−30] While there are a few monolayer sheets of metal–organic and coordination polymers known,[15−17,19,21] to the best of our knowledge, transmetalations at the single-sheet level have not yet been reported. Also for the famous Lehn grids[31,32] and for tpy-based linear metal–organic polymers,[33−35] such reactions were not yet reported. While not directly related, at least for surface-bound tpy metal complexes, removal of metal cations has in fact been observed.[36] We consider such experiments particularly interesting because, apart from the above-mentioned exchange in MOFs, where area control of the transmetalation has not been achieved and may in fact be difficult to achieve, monolayer sheets offer random as well as area-specific exchange. The latter should be possible at least on the length scale accessible by patterning strategies from photolithography,[37] microcontact printing, and dip-pen nanolithography.[38,39] Thus, if transmetalation with metal–organic sheets can be brought about, it provides a novel and particularly facile approach to modify their integral network structure and thus composition, which sets this method apart from the more common method of sheet modification by surface decoration and also from substitutional doping.[40] Furthermore, looking at transmetalation of metal–organic sheets with the eyes of a polymer chemist, this process converts a homosheet into a heterosheet, whereby the latter is a two-dimensional analogue of random copolymers (for random exchange) or block copolymers (for area-specific exchange). Thus, the attempts described here help pave the way into a new dimensionality of polymer chemistry.

We present here a study of the successful transmetalation of Zn^{2+} in **S1**(Zn^{2+}) and **S2**(Zn^{2+}) mainly to Fe^{2+} but also to Co^{2+} and Pb^{2+} within cm^2-sized monolayer sheets. The transmetalation is carried out with sheets, which have approximately 63 and 70%, respectively, of $[Zn(tpy)_2]^{2+}$ netpoints while they are supported on 285 nm SiO_2/Si, 300 nm Au/10 nm Ti/Si, glass, and quartz. Transmetalation is investigated by UV/vis and fluorescence spectroscopy, X-ray photoelectron spectroscopy (XPS), Raman spectroscopy/microscopy, optical microscopy (OM), atomic force microscopy (AFM), and neutron reflectivity (NR). Finally, successful transmetalation is illustrated by spanning the sheet obtained after the Zn/Fe conversion over 20 × 20 μm^2 sized holes. In a second part, we describe how by area-selective transmetalation sheet **S1**(Zn^{2+}) after appropriate masking is converted from a homogeneous sheet into a two-dimensional block copolymer (2DBP) consisting of alternating Zn^{2+}- and Fe^{2+}-based netpoints with predesigned size and shape. Photophysical properties of the different blocks are investigated, and the monolayer nature of the 2DBP is demonstrated by suspending it again over 20 × 20 μm^2 sized holes, which requires on the order of 10^7 monomer molecules per hole. Last but not least, a structure of **S1**(Met^{2+}) is proposed by density functional theory (DFT) calculation, and a possible transmetalation mechanism is suggested based on the proposed structure.

2. RESULTS

2.1. Transmetalation in Monolayer Sheets. The experiments were started with sheet **S1**(Zn^{2+}) for which not only much experience was available[17] but also the netpoints were expected to be among the weakest if studies on the binding constant of $[Met(tpy)_2]^{2+}$ complexes in dependence of the metal ions in solution can be qualitatively applied to networks.[41] N 1s XPS studies confirmed that 63% of all tpy units were involved in $[Zn(tpy)_2]^{2+}$ complexes. A sheet was transferred from the air/water interface onto a several cm^2-sized quartz slide and after drying partially immersed into an aqueous 10 mmol L^{-1} solution of $(NH_4)_2Fe(SO_4)_2$ (at pH ∼6.4) for 1 h at room temperature. Figure 2a–c shows photographs of the fluorescing sheet **S1**(Zn^{2+}) on quartz (excitation at λ = 287 nm), the dipping procedure, and the result after dipping. Figure 2d compares UV–vis (blue) and the fluorescence spectra (purple) of sheet **S1**(Zn^{2+}) with that of the dipped area [UV–vis (black); no fluorescence]. Both the UV–vis (π–π^* transition of tpy at 278 nm) and the fluorescence spectra (blue emission at λ = 435 nm) confirm that **S1**(Zn^{2+}) has actually been transferred onto the entire slide. Interestingly, the UV–vis spectrum of the dipped area shows a signal at λ = 578 nm, which is reminiscent of the metal-to-ligand charge transfer (MLCT) band observed earlier for **S1**(Fe^{2+}) and characteristic for $[Fe(tpy)_2]^{2+}$ netpoints. Thus, tentatively we propose that the metal ion exchange has taken place, in line with the absence of fluorescence in the dipped area [sheet **S1**(Fe^{2+}) is nonfluorescent].[16]

dx.doi.org/10.1021/ja501849y | J. Am. Chem. Soc. 2014, 136, 6103–6110

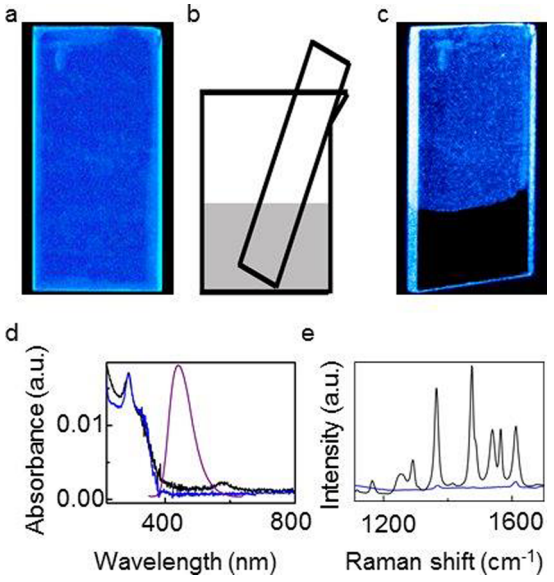

Figure 2. Characterization of **S1**(Zn^{2+}) before and after transmetalation. Photographs of (a) fluorescent monolayer sheet **S1**(Zn^{2+}) on quartz (3.3 cm × 1.4 cm), (b) dipping procedure to affect transmetalation, and (c) the sheet after 1 h partial exposure to a 10 mmol L^{-1} $(NH_4)_2Fe(SO_4)_2$ solution in water. (d) UV−vis (blue) and fluorescence spectra (purple) of starting sheet **S1**(Zn^{2+}) and UV−vis spectrum (black) of the product sheet. (e) Raman spectra of the starting (blue) and product sheet (black) on thin borosilicate glass slides in transmission mode.

The proposed transmetalation is confirmed by XPS. Figure 3a shows the XP spectra of Zn $2p_{3/2}$, Fe $2p_{3/2}$, and N 1s signals from starting sheet **S1**(Zn^{2+}) on 300 nm Au/10 nm Ti/Si

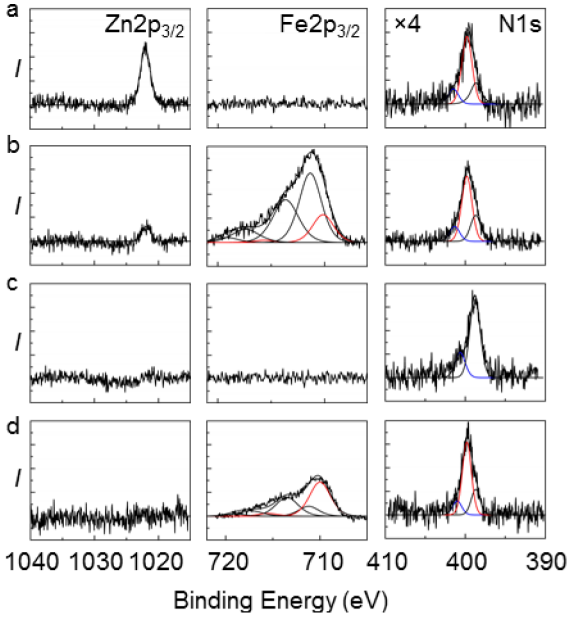

Figure 3. X-ray photoelectron spectra (XPS) proving transmetalation. Zn $2p_{3/2}$, Fe $2p_{3/2}$, and N 1s signals of **S1**(Zn^{2+}) (a) before and (b) after 1 h immersion in 10 mmol L^{-1} $(NH_4)_2Fe(SO_4)_2$, (c) after 1 h immersion in 0.1 mol L^{-1} HCl solution, and (d) after 1 h immersion in 10 mmol L^{-1} $(NH_4)_2Fe(SO_4)_2$ followed by 1 h immersion in 0.1 mol L^{-1} HCl solution. The intensity (I) of the N 1s signal was expanded by a factor of 4.

substrate. The N 1s signal contains three peaks at 398.7, 399.8, and 401.9 eV, which are due to unmodified tpy, $[Zn(tpy)_2]^{2+}$, and $[Zn(tpy)]^{2+}$ or protonated tpy, respectively.[17] For the assignment of the other signals, see ref 17. The fraction of the 399.8 eV peak intensity on total N 1s signal intensity is ∼63%. This value represents the conversion reached during sheet synthesis at the air/water interface and is therefore an important reference point in the attempted transmetalation.[17] Figure 3a shows the Zn 2p signal to be more intense than expected from the N 1s $[Zn(tpy)_2]^{2+}$ signal. Thus, there is residual Zn^{2+} salt adhered to the sheet not engaged in $[Zn(tpy)_2]^{2+}$ netpoints. Figure 3b was recorded after sheet **S1**(Zn^{2+}) had been exposed to the Fe salt solution for 1 h, a time period during which the intensity of the MLCT band had already long reached its maximum value. The N 1s $[Met(tpy)_2]^{2+}$ intensity on total N 1s was monitored over the entire transmetalation period and found to remain practically constant (Figure 4). Note that the 399.8 eV peak is characteristic for the

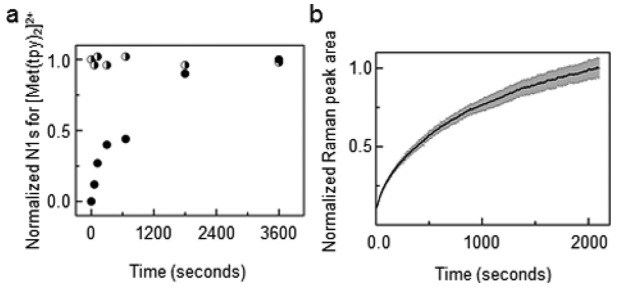

Figure 4. Transmetalation process monitored by XPS and Raman analysis. (a) Normalized fractional intensity of N 1s XPS signal assigned to $[Met(tpy)_2]^{2+}$ versus time. Half circles: **S1**(Zn^{2+}) exposed to 10 mmol L^{-1} Fe^{2+} for various times. Full circles: **S1**(Zn^{2+}) exposed to 10 mmol L^{-1} Fe^{2+} for various times, followed by 1 h immersion in 0.1 mol L^{-1} HCl. (b) Normalized peak area of the ν(phenyl-tpy) Raman mode. Error bars represent +/− the standard deviation.

structural motif $[Met(tpy)_2]^{2+}$ but not sensitive to the nature of the metal ion. Its constancy therefore neither proves nor disproves transmetalation but allows concluding that neither transmetalation nor immersing into HCl changes the amount of monomers in the sheet.

Besides the N 1s signal, Figure 3b also shows a Zn 2p signal and an intense Fe peak, part of which is assigned to Fe^{2+} (no further specification).[17] To approach the issue of transmetalation, it was first tested whether all Zn^{2+}, which concerns the ones involved in $[Zn(tpy)_2]^{2+}$ units and the ones contained in not further identified "impurities", can be removed from starting sheet **S1**(Zn^{2+}). Immersion of this sheet into 0.1 mol L^{-1} HCl for 1 h resulted in an almost complete disappearance of the $Zn2P_{3/2}$ signal (Figure 3a,c); also, the N 1s $[Zn(tpy)_2]^{2+}$ signal vanished, just leaving the signature of bare tpy and protonated tpy behind. With this information at hand, the supposedly transmetalated sheet **S1**(Zn^{2+}) [after transmetalation: **S1**(Fe^{2+})] was exposed to the same acidic conditions. If the exchange has taken place, the sheet is not **S1**(Zn^{2+}) anymore but rather **S1**(Fe^{2+}), and it was expected that, while the Zn signal should disappear altogether, the fraction of the N 1s signal due to $[Met(tpy)_2]^{2+}$ should remain constant; Fe^{2+} cannot be removed from $[Fe(tpy)_2]^{2+}$ under such conditions. Such observation would allow conclusion that this signal fraction is actually solely due to $[Fe(tpy)_2]^{2+}$, and thus, transmetalation has actually taken place. As the comparison of

dx.doi.org/10.1021/ja501849y | J. Am. Chem. Soc. 2014, 136, 6103−6110

Figure 3b,d shows, this expectation turned out to be true. Not only did the Zn signal vanish but also the $[Met(tpy)_2]^{2+}$ intensity remained constant. We also monitored the progress of transmetalation by XPS (ex situ). Sheet **S1**(Zn^{2+}) was treated for 1, 2, 5, 11, 30, and 60 min with the Fe salt solution before immersing the product into the acid solution for 1 h. Subsequent XPS analysis showed that the $[Met(tpy)_2]^{2+}$ fraction of the N 1s signal gradually increases until it reaches 63% (Figure 4a).

The Fe signals in Figure 3b,d are worth mentioning. As already reported earlier,[17] comparing the two signals with one another provides insight into the efficiency of the immersing procedure in terms of removal of unwanted Fe-based impurities (of which there are many). While in Figure 3b the Fe^{2+} signal is among the weakest, in 3d it is actually the most intense. Obviously iron oxide and other Fe impurities can be removed to a considerable degree, which will stimulate further experimentation into sheet-cleaning procedures.

The exchange process was further investigated by Raman spectroscopy. Figure 2e compares the Raman spectra in transmission mode of **S1**(Zn^{2+}) and the proposed product sheet **S1**(Fe^{2+}). Raman and resonance Raman spectroscopy of bis-tpy complexes (metal ions: Fe^{2+}, Ru^{2+}, Zn^{2+}) is the topic of various publications.[42−48] The Fe^{2+} and Ru^{2+} complexes show MLCT transitions in the visible part of the electromagnetic spectrum. When the Raman excitation wavelength (532 nm in the present case) is in the same range as these electronic transitions, Franck−Condon active vibrations become enhanced (resonance Raman effect).[49] In contrast, Zn^{2+} has d^{10} configuration (full electron shell) and does not show MLCT transitions.[45]

The aromatic in-plane vibration at 1610 cm^{-1} and the tpy ring breathing mode ν(phenyl-tpy) at 1367 cm^{-1} are the only Raman bands observed for **S1**(Zn^{2+}). The resonance Raman spectrum of the **S1**(Fe^{2+}) additionally shows strong bands at 1473 and 1163 cm^{-1} (assigned to tpy vibrations) as well as at 1532 and 1363 cm^{-1} (assigned to vibrations, with significant involvement of the benzene ring attached to the 4′-position of the tpy ligand). This indicates delocalization of the MLCT excited state over the connected ring. The ν(phenyl-tpy) mode is slightly shifted to 1363 cm^{-1}. Since this mode involves strong phenyl-tpy bond stretching, its position can be shifted depending on the binding situation to the metal center.[45] More detailed band assignments for similar resonant and nonresonant Raman spectra of Ru(II) and Zn(II) complexes can be found in the literature.[43,45,47] Moreover, a series of Raman spectra were acquired after placing a drop of freshly prepared Fe salt solution (approximately 0.05 mL, 60 000-fold molar excess) on a sheet **S1**(Zn^{2+}) on glass with an acquisition time of 10 s per spectrum (see Supporting Information movie 1). The intensities of the Raman bands reached their maximum at approximately 30 min. Figure 4b shows the time-dependent evolution of the transmetalation based on the peak area of the ν(phenyl-tpy) mode. In principle, the experiment can be stopped at any reaction conversion, which opens the door to study conversion-dependent properties of the nanosheets. Note that this cannot be realized by sheet synthesis at an air−water interface.

Transmetalation of **S1**(Zn^{2+}) to **S1**(Fe^{2+}) was also followed by OM, AFM, and NR. Figure 5a shows an OM image of a vertically transferred **S1**(Zn^{2+}) on 285 nm SiO_2. A random crack, most likely formed during transfer, created the necessary contrast to follow sheet topography during transmetalation.

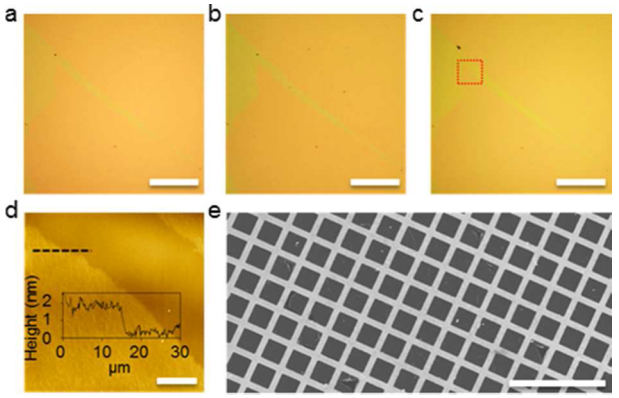

Figure 5. Microscopic images of sheets prepared by transmetalation. Optical microscopy images of **S1**(Zn^{2+}) on 285 nm SiO_2 (a) before and (b) after 1 h immersion in 10 mmol L^{-1} $(NH_4)_2Fe(SO_4)_2$ and (c) after an additional 1 h immersion in 0.1 mol L^{-1} HCl sonication bath at ∼20 W. (d) AFM topographic image of the red square inserted in (c) with a height profile. (e) TEM image of freely suspended **S1**(Fe^{2+}) sheet synthesized by transmetalation of **S1**(Zn^{2+}) over a copper grid. Scale bars: 200 μm (a−c); 20 μm (d); 100 μm (e).

The interference color stayed homogeneous throughout transmetalation (Figure 5b) and subsequent zinc removal with HCl (Figure 5c), reflecting homogeneity of sheet thickness during the chemical processes. Note that the lateral size of the sheet also stays unchanged during the process. The color contrast at the crack helped direct an AFM tip to sheet edges to determine sheet thickness. Height profiles gave h_{AFM} = 1.5 nm (Figure 5d), which corresponds well with a monolayer thickness (see below).[16] While AFM gives the local thickness determined from small areas (normally scan size is less than 100 μm × 100 μm), NR gives an averaged thickness over much larger areas (here ∼2 cm × 10 cm). NR applied to **S1**(Zn^{2+}) before and after the transmetalation with subsequent immersion in 0.1 M HCl for 1 h gave h_{NR} = 1.34 and 1.35 nm, respectively (see Supporting Information Figure S1). The consistency of the number of $[Met(tpy)_2]^{2+}$ (XPS), the number of monomers (N 1s intensity by XPS), the lateral size, and thickness of the sheet before and after the chemical process indicate that there will only be minor molecular structure changes during the transmetalation if any.

After all of these analyses, we set out to provide a final proof for transmetalation. Sheet **S1**(Fe^{2+}) directly synthesized from monomer and Fe salt is robust enough to be spanned over 20 × 20 μm^2 sized holes of an electron microscopy grid.[16] The same should of course apply to a sheet **S1**(Fe^{2+}) obtained from transmetalation. Because the transmetalation was done on a solid support, a transfer technique[50] had to be applied in order to create a freely suspended sheet on a grid (see Supporting Information Figure S2). The TEM image shows the transmetalated sheet spanned over holes (note the few ruptures), thus proving the mechanical coherence.

2.2. Two-Dimensional Analogues of Block Copolymer.

In combination with patterning techniques, such as photolithography, transmetalation reactions on sheets can, in principle, be performed in predetermined areas, opening exciting options in molecular structure design. Figure 6a schematically shows the procedure to obtain a monolayer sheet with alternating stripes of Zn-based netpoints (for **S1**(Zn^{2+})) and Fe-based netpoints (for **S1**(Fe^{2+})). The experiment was started with **S1**(Zn^{2+}) on 285 nm SiO_2/Si or 300 nm Au/mica.

dx.doi.org/10.1021/ja501849y | J. Am. Chem. Soc. 2014, 136, 6103−6110

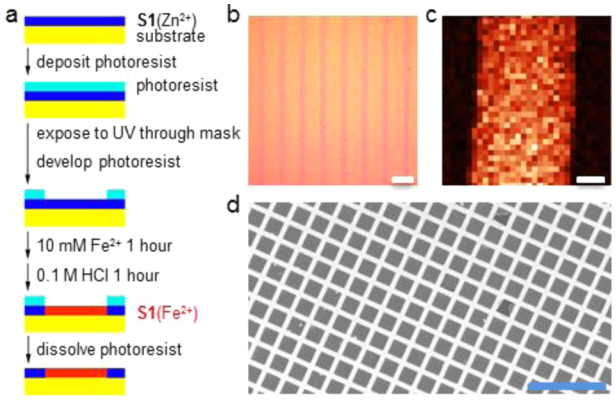

Figure 6. Two-dimensional analogue of a block copolymer (2DBP). (a) Schematic process to create 2DBP. Optical microscopy (b) and Raman microscopy (c) images of 2DBP on 285 nm SiO_2/Si. (d) TEM image of freely suspended 2DBP over a copper grid. Scale bars: 100 μm (b); 5 μm (c); 100 μm (d).

This sample was spin-coated with a layer of photoresist and subsequently exposed to UV irradiation through predesigned patterns of a mask. This resulted in a layer of patterned photoresist on the sample after conventional photoresist development. The above transmetalation protocol was then applied to the exposed sheet area to transfer the pattern of the mask to the sheet. After completion of transmetalation the photoresist was removed. Figure 6b shows the OM image of such a sheet. The reddish lines with a width of about 20 μm are **S1**(Fe^{2+}) and the ones between with a width of around 80 μm are **S1**(Zn^{2+}), based on the experimental design. The color contrast between the sheet areas with the different netpoints is probably caused by differences in refractive index. This should lead to different interference colors despite the same thickness. Note that the color difference cannot be distinguished by OM when transmetalated areas are not large enough for OM resolution or when different netpoints are randomly dispersed. The chemical compositions of the alternating structures were further confirmed by Raman imaging experiments. The Raman spectra of the **S1**(Zn^{2+}) and **S1**(Fe^{2+}) resemble the ones of **S1**(Zn^{2+}) and **S1**(Fe^{2+}) prepared at the air–water interface (Figure 2e and Supporting Information Figure S3), validating the netpoint assignments. The Raman intensity image for the band at 1473 cm^{-1} in Figure 6c was obtained when scanning the excitation laser across one of the reddish lines in Figure 6b. Clear contrast between the Fe-based and the Zn-based netpoints was observed, indicating a sharp edge between the areas with Zn/Fe-based netpoints. To prove that this patterned sheet can carry its own weight, it was released from the supporting substrate and freely suspended over 20 × 20 μm^2 sized holes by PMMA-mediated transfer. Practically all holes of the grid were homogeneously spanned, which becomes apparent by visual inspection of the few ruptures present (Figure 6d). This proves the sheet's mechanical coherence and its high enough strength to be considered as an independent entity. Looking at such a sheet with the eyes of a polymer chemist, one may (loosely) consider it as a monolayer 2DBP.

Next, the transparency and spectroscopic properties of the two different blocks of "2DBP" were investigated. While **S1**(Fe^{2+}) absorbs 0.5% of visible light and is nonfluorescent, **S1**(Zn^{2+}) is 100% transparent in visible light and emits in blue under UV irradiation (Figure 2d). The fluorescence quantum yield (QY) of **S1**(Zn^{2+}) is about 7%, while that of $[Zn_3(\mathbf{1})]^{2+}$ complexes in diluted CH_2Cl_2 is about 14%. Thus, the QY decreased by 50% for the sheet, which is normal when comparing tpy complexes (emissive species in light-emitting devices) in solution and in the solid state.[51] Note that tpy derivatives so far investigated in film form required a solid support. In contrast, **S1**(Zn^{2+}) is a free-standing sheet,[17] which may be an attractive feature for fluorescence-based sensing because of lack of interference by the substrate.

2.3. DFT Calculations. Experiments to unravel the molecular structure of **S1**(Met^{2+}) with atomistic detail are difficult and time-consuming. To nevertheless approach this important matter, existing data are complemented by DFT calculations and theoretical considerations,[52,53] leading to the detailed model for **S1**(Fe^{2+}) shown in Figure 7. It is similar to the idealized structure shown in Figure 1 but suggests locations for the SO_4^{2-} anions and for the 66% metalated netpoints. SO_4^{2-} can be incorporated within the sheets for conversion rates below 66%. Afterward, it must be adsorbed on the sheet surface, which is found to be energetically less favorable, even if a few explicit water molecules are included in the model. This rationalizes the conversion rate (~66%) observed in experiment with SO_4^{2-} as counterions.[17] It is also noteworthy that this also suggests a potentially important role for the anion in sheet synthesis; a similar observation has been made for self-assembly of circular helicates.[54] In the proposed model, nonmetalated tpy bends out of the plane of the sheet, such that the two tpys of a potential link are found on opposite sides of the sheet. These tpys are in a different conformation from the bound tpys. The flexibility of the proposed structure allows the two metalated tpys of a link to become orthogonal, which is not possible in the fully converted structure and might facilitate metal exchange. Furthermore, sheet thickness increases from ~8 Å (idealized, fully converted structure) to ~12 Å, which is also in good agreement with the experimental value.

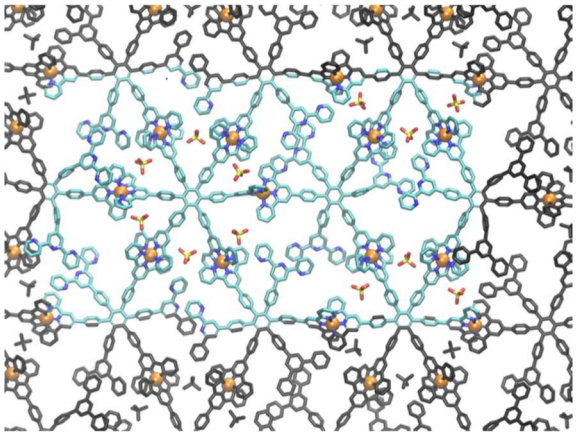

Figure 7. DFT structure of **S1**(Fe^{2+}) which minimizes Coulombic repulsion at 66% metalation and possesses isotropic mechanical strength. Color code: light blue rectangle in the center, unit cell; dark blue, nitrogen; golden spheres, Fe^{2+}; yellow-orange tetrahedrons, SO_4^{2-} counterions.

Studying these sheets with partial conversion, we find that it is energetically favorable to maximize the distance between metalated links. Equivalently, one could say that the locations of nonmetalated links, named defects in the following, are correlated. This is key to explain the experimentally derived[55] in-plane elastic modulus of $E^{2D} = 22 \pm 3$ N m^{-1} and to arrive at the presented model, which has a certain regularity in the

dx.doi.org/10.1021/ja501849y | J. Am. Chem. Soc. 2014, 136, 6103–6110

distribution of defects. Indeed, it is possible to describe the idealized system with 100% conversion as a central force triangular 2D lattice, with monomers being the vertices and the tpy−tpy links the edges. In percolation theory, which includes the study of random defects on such lattices, the rigidity bond percolation threshold for this lattice has been derived as ∼0.65;[56] that is, for the typically observed experimental conversion ratios, no macroscopic stiffness would remain if defects were truly random. As the reported experimental value is significant and reaches roughly 50% of the computed DFT result for an idealized, fully metalated sheet ($E^{2D} \sim 37.0$ N m^{-1}, Poisson ratio 0.36), the experimental defect distribution cannot be random, consistent with the computed correlation in defect location.

At 66% conversion, minimizing the number of nearest neighbor metalated links is equivalent to ordering defects such that only one link per lattice triangle is defective. Imposing this rule leads to short, but not necessarily long-range defect order. DFT calculations are performed on an isotropic periodic model that follows this rule, namely, the rhombille tiling, shown in Figure 7. It has favorable energetics and leads to a computed elastic modulus of $E^{2D} \sim 16.1$ N m^{-1} and a Poisson ratio of 0.62. The elastic modulus is in good agreement with the experimental nanoindentation results,[55] but this becomes clear only after reinterpretation of the measured force/displacement data with the computed Poisson ratio. Indeed, the published[17] $E^{2D} = 22 \pm 3$ N m^{-1} was derived from the data based on the assumption of a Poisson ratio of 0.35 but must be revised to $E^{2D} = 17.2$ N m^{-1} if the computed Poisson ratio (0.62) is employed instead. The revised E^{2D} is in excellent agreement with the DFT result. We note that the Poisson ratio of graphene (0.15)[55,57] is much lower as a result of the stiff bending (angular) terms, absent in **S1**(Fe^{2+}), while a triple honeycomb lattice model with only central forces[58] can be parametrized to yield any Poisson ratio between 1/3 and 1. Finally, we have used a variant of the latter model to show that also randomized models that follow the rule of one weak link per triangle exhibit elastic properties that are very similar to the rhombille lattice, suggesting that this model is robust.

3. DISCUSSION

Last but not least, the process of transmetalation deserves a comment. Based on the analytical results provided, it is firm to conclude that Zn^{2+} connecting the two tpy units in the $[Zn(tpy)_2]^{2+}$ netpoints of sheets **S1**(Zn^{2+}) and **S2**(Zn^{2+}) can be transmetalated by Fe^{2+} and likely also by other metal ions, as suggested by the successful exchanges with the rather different metal ions Pb^{2+} and Co^{2+} (see Supporting Information Figures S4 and S5). It is noted that the metal ions to be transmetalated into a sheet are being used in huge excess. Following the principle of Le Chatelier and given the dynamic equilibrium nature of the bond between Zn^{2+} and tpy, transmetalation is an obvious encounter. It is further favored by the strength of Fe/Pb/Co-tpy bonds which tend to be higher than that of Zn-tpy bond.[59] Since parent monomer **S1** on SiO_2 is removed to a substantial degree when exposed to aqueous Fe^{2+} or Zn^{2+} solutions (as judged by XPS N 1s intensity; not further described), the fact that transmetalation is observed without loss of monomer indicates that it proceeds netpoint by netpoint and not by a scenario, where monomers are entirely disconnected from the rest of the initial network before the new metal ions place themselves into previous netpoints (see Supporting Information Figure S6). The transmetalation conversion of **S1**(Zn^{2+}) with Fe^{2+} is on the order of 63%, which resembles the fraction of $[Zn(tpy)_2]^{2+}$ netpoints present in the sheet. While this may be by coincidence, it may also indicate that it is exactly the Zn-based netpoints that are quantitatively being transmetalated. At first glance, it is astounding why the remaining tpy ligands should not get involved in netpoint formation if there are so many metal ions around. The DFT molecular structure, however, offers a plausible explanation here. The $[Zn(tpy)_2]^{2+}$ netpoints in **S1**(Zn^{2+}) hold the two tpy at close distance, while in the defects of the sheet (defects: $[Zn(tpy)]^{2+}$/protonated tpy or bare tpy[17]), the tpys are far away from each other (see Figure 7, in which defects are only shown as bare tpys for simplicity). Thus, exchange at netpoints could be associated with less activation barrier than pulling two distant tpy together into a $[Met(tpy)_2]^{2+}$ netpoint. There is another observation which sheds some light on the exchange mechanism. While sheet **S1**(Pb^{2+})/**S2**(Pb^{2+}) synthesized at the air/water interface from monomer and Pb^{2+} contains no more than 23%/14% of regular $[Pb(tpy)_2]^{2+}$ netpoints, after transmetalation of **S1**(Zn^{2+})/**S2**(Zn^{2+}) with Pb^{2+}, again 63%/70% such netpoints are found (by XPS) (see Supporting Information Figures S4, S7, and S8), which despite the considerable error bar on XPS measurements seems to resemble the fraction of $[Zn(tpy)_2]^{2+}$ netpoints initially present! If this assertion holds true, zinc in the starting sheet **S1**(Zn^{2+}) favors its own exchange. To further see the generality of the reaction, transmetalation was also proven for the sheet **S2**(Zn^{2+}) with Fe^{2+} and Co^{2+} (see Supporting Information Figures S9 and S10). Finally, according to in situ Raman spectroscopy monitoring described above, transmetalation can be stopped at practically any conversion. Assuming this exchange to be random, it provides access to sheets with a random distribution of two different metals in the netpoints. In the terminology of linear polymers, this is reminiscent of random copolymers, thus we are dealing with random metal−organic sheet copolymers until transmetalation is complete. As the process proceeds on a time scale of tens of minutes, it can be controlled easily.

4. CONCLUSION

In summary, when starting from a monolayer metal−organic sheet such as **S1**(Zn^{2+}) containing ∼63% of $[Zn(tpy)_2]^{2+}$ netpoints, its zinc ions can be completely exchanged (transmetalated) by Fe^{2+}. This is a very mild process which is not restricted to Fe^{2+}. There is evidence that this exchange takes place at the location of the Zn. In accordance with this proposal is the finding that the sheets after transmetalation can still be spanned over 20 × 20 μm^2 holes, suggesting an unaltered mechanical integrity. Transmetalation is likely to proceed in random fashion and thus provides access to sheet analogues of random linear copolymers. If driven to completion and with application of conventional photoresist technology, predesigned patterns of masks can be 1:1 transferred into sheets consisting of domains with zinc-based netpoints and those with Fe-based netpoints. If masks with stripe patterns are employed, sheets are obtained after transmetalation, which can be viewed as the two-dimensional analogues of linear block copolymers. DFT calculations provide a molecular model of the sheet **S1**(Fe^{2+}), which suggests a regular pattern of 66% operational and 33% non-operational netpoints distributed over the sheet. This model explains why not all tpy units are involved in $[Fe(tpy)_2]^{2+}$ netpoints: 33% of them are too far away from one another to allow for the simultaneous binding of two tpys to

dx.doi.org/10.1021/ja501849y | J. Am. Chem. Soc. 2014, 136, 6103−6110

one metal ion. The model further estimates an in-plane elastic constant of 16.1 N m^{-1}, which is in good agreement with the experimental value of 17.2 N m^{-1} after its correction for a more appropriate Poisson ratio. It further explains why a sheet with a conversion of 63% can exhibit a mechanical strength at all, despite the fact that such conversion is below the percolation threshold of 66% for networks with triangular connectivity: This threshold applies to networks with random defects, and the observed mechanical strength suggests therefore order in our sheet. It is noted that the transmetalation is particularly easy to perform. Simple dipping followed by a few rinses with 0.1 mol L^{-1} HCl already provides the product sheet. This represents an advance in monolayer sheet chemistry, property modification, and patterning, which has the potential to reach out into molecular electronics, device fabrication, nanoscale synthesis, imaging, and sensing.

■ ASSOCIATED CONTENT

Supporting Information

Experimental methods, data analysis of neutron reflectivity, supplementary XPS figures, and DFT input file. This material is available free of charge via the Internet at http://pubs.acs.org.

■ AUTHOR INFORMATION

Corresponding Authors

zhikun.zheng@mat.ethz.ch
dieter.schlueter@mat.ethz.ch

Notes

The authors declare no competing financial interest.

■ ACKNOWLEDGMENTS

We thank Prof. G. Wegner (MPI-P, Mainz) for useful advice, Prof. A. Rossi (ETHZ) for access to XPS, Prof. N. Spencer (ETHZ) for access to AFM, and the ETH cleanroom facility FIRST. We thank W. Dai for help with synthesis. This work was supported by ETH Zürich (ETH-26 10-2) and the Swiss National Science Foundation. Calculations were enabled by a grant from the Swiss National Supercomputer Centre (CSCS) under project ID s441.

■ REFERENCES

(1) Novoselov, K. S.; Jiang, D.; Schedin, F.; Booth, T. J.; Khotkevich, V. V.; Morozov, S. V.; Geim, A. K. *Proc. Natl. Acad. Sci. U.S.A.* **2005**, *102*, 10451−10453.

(2) Xu, M.; Lian, T.; Shi, M.; Chen, H. *Chem. Rev.* **2013**, *113*, 3766−3798.

(3) Unarunotai, S.; Murata, Y.; Chialvo, C. E.; Mason, N.; Petrov, I.; Nuzzo, R. G.; Moore, J. S.; Rogers, J. A. *Adv. Mater.* **2010**, *22*, 1072−1077.

(4) Perepichka, D. F.; Rosei, F. *Science* **2009**, *323*, 216−217.

(5) Ma, R.; Sasaki, T. *Adv. Mater.* **2010**, *22*, 5082−5104.

(6) Park, S.; Ruoff, R. S. *Nat. Nanotechnol.* **2009**, *4*, 217−224.

(7) Levendorf, M. P.; Kim, C. J.; Brown, L.; Huang, P. Y.; Havener, R. W.; Muller, D. A.; Park, J. *Nature* **2012**, *488*, 627−632.

(8) Ci, L.; Song, L.; Jin, C.; Jariwala, D.; Wu, D.; Li, Y.; Srivastava, A.; Wang, Z. F.; Storr, K.; Balicas, L.; Liu, F.; Ajayan, P. M. *Nat. Mater.* **2010**, *9*, 430−435.

(9) Liu, Z.; Ma, L.; Shi, G.; Zhou, W.; Gong, Y.; Lei, S.; Yang, X.; Zhang, J.; Yu, J.; Hackenberg, K. P.; Babakhani, A.; Idrobo, J.-C.; Vajtai, R.; Lou, J.; Ajayan, P. M. *Nat. Nanotechnol.* **2013**, *8*, 119−124.

(10) Lu, J.; Zhang, K.; Liu, X. F.; Zhang, H.; Sum, T. C.; Neto, A. H. C.; Loh, K. P. *Nat. Commun.* **2013**, *4*, 2681.

(11) Turchanin, A.; Gölzhäuser, A. *Prog. Surf. Sci.* **2012**, *87*, 108−162.

(12) Kissel, P.; Erni, R.; Schweizer, W. B.; Rossell, M. D.; King, B. T.; Bauer, T.; Goetzinger, S.; Schlueter, A. D.; Sakamoto, J. *Nat. Chem.* **2012**, *4*, 287−291.

(13) Uribe-Romo, F. J.; Dichtel, W. R. *Nat. Chem.* **2012**, *4*, 244−245.

(14) Bhola, R.; Payamyar, P.; Murray, D. J.; Kumar, B.; Teator, A. J.; Schmidt, M. U.; Hammer, S. M.; Saha, A.; Sakamoto, J.; Schlüter, A. D.; King, B. T. *J. Am. Chem. Soc.* **2013**, *135*, 14134−14141.

(15) Kambe, T.; Sakamoto, R.; Hoshiko, K.; Takada, K.; Miyachi, M.; Ryu, J.-H.; Sasaki, S.; Kim, J.; Nakazato, K.; Takata, M.; Nishihara, H. *J. Am. Chem. Soc.* **2013**, *135*, 2462−2465.

(16) Bauer, T.; Zheng, Z.; Renn, A.; Enning, R.; Stemmer, A.; Sakamoto, J.; Schlűter, A. D. *Angew. Chem., Int. Ed.* **2011**, *50*, 7879−7884.

(17) Zheng, Z.; Ruiz-Vargas, C. S.; Bauer, T.; Rossi, A.; Payamyar, P.; Schütz, A.; Stemmer, A.; Sakamoto, J.; Schlüter, A. D. *Macromol. Rapid Commun.* **2013**, *34*, 1670−1680.

(18) (a) Payamyar, P.; Kaja, K.; Ruiz-Vargas, C.; Stemmer, A.; Murray, D. J.; Johnson, C.; King, B. T.; Schiffmann, F.; VandeVondele, J.; Renn, A.; Götzinger, S.; Ceroni, P.; Schütz, A.; Lee, L.-T.; Zheng, Z.; Sakamoto, J.; Schlüter, A. D. *Adv. Mater.* **2013**, *26*, 2052−2058. (b) Chen, Y.; Li, M.; Payamyar, P.; Zheng, Z.; Sakamoto, J.; Schlüter, A. D. *ACS Macro Lett.* **2014**, *3*, 153−158.

(19) Makiura, R.; Motoyama, S.; Umemura, Y.; Yamanaka, H.; Sakata, O.; Kitagawa, H. *Nat. Mater.* **2010**, *9*, 565−571.

(20) Schultz, M. J.; Zhang, X.; Unarunotai, S.; Khang, D.-Y.; Cao, Q.; Wang, C.; Lei, C.; MacLaren, S.; Soares, J. A. N. T.; Petrov, I.; Moore, J. S.; Rogers, J. A. *Proc. Natl. Acad. Sci. U.S.A.* **2008**, *105*, 7353−7358.

(21) (a) Gallego, A.; Hermosa, C.; Castillo, O.; Berlanga, I.; Gómez-García, C. J.; Mateo-Martí, E.; Martínez, J. I.; Flores, F.; Gómez-Navarro, C.; Gómez-Herrero, J.; Delgado, S.; Zamora, F. *Adv. Mater.* **2013**, *25*, 2141−2146. (b) Amo-Ochoa, P.; Welte, L.; González-Prieto, R.; Sanz Miguel, P. J.; Gómez-García, C. J.; Mateo-Martí, E.; Delgado, S.; Gómez-Herrero, J.; Zamora, F. *Chem. Commun.* **2010**, *46*, 3262−3264. (c) Bauer, T.; Schlüter, A. D.; Sakamoto, J. *Synlett* **2010**, *6*, 877−880. (d) Sakamoto, J. Habilitation Thesis, ETH Zurich, Switzerland, 2012.

(22) Burrows, A. D. *CrystEngComm* **2011**, *13*, 3623−3642.

(23) Nam, K. T.; Shelby, S. A.; Choi, P. H.; Marciel, A. B.; Chen, R.; Tan, L.; Chu, T. K.; Mesch, R. A.; Lee, B.-C.; Connolly, M. D.; Kisielowski, C.; Zuckermann, R. N. *Nat. Mater.* **2010**, *9*, 454−460.

(24) Zheng, Y.; Zhou, H.; Liu, D.; Floudas, G.; Wagner, M.; Koynov, K.; Mezger, M.; Butt, H. J.; Ikeda, T. *Angew. Chem., Int. Ed.* **2013**, *52*, 4845−4848.

(25) Das, S.; Kim, H.; Kim, K. *J. Am. Chem. Soc.* **2009**, *131*, 3814−3815.

(26) Tian, J.; Saraf, L. V.; Schwenzer, B.; Taylor, S. M.; Brechin, E. K.; Liu, J.; Dalgarno, S. J.; Thallapally, P. K. *J. Am. Chem. Soc.* **2012**, *134*, 9581−9584.

(27) Mircea, D.; Jeffrey, R. L. *J. Am. Chem. Soc.* **2007**, *129*, 11172−11176.

(28) Mi, L.; Hou, H.; Song, Z.; Han, H.; Xu, H.; Fan, Y.; Ng, S. W. *Cryst. Growth Des.* **2007**, *7*, 2553−2561.

(29) Mukherjee, G.; Biradha, K. *Chem. Commun.* **2012**, *48*, 4293−4295.

(30) Shultz, A. M.; Sarjeant, A. A.; Farha, O. K.; Hupp, J.; Nguyen, S. T. *J. Am. Chem. Soc.* **2011**, *133*, 13252−13255.

(31) Garcia, A. M.; Romero-Salguero, F. J.; Bassani, D. M.; Lehn, J.; Baum, G.; Fenske, D. *Chem.—Eur. J.* **1999**, *5*, 1803−1808.

(32) Barboiu, M.; Vaughan, G.; Graff, R.; Lehn, J. *J. Am. Chem. Soc.* **2003**, *125*, 10257−10265.

(33) Schubert, U. S.; Eschbaumer, C. *Angew. Chem., Int. Ed.* **2002**, *41*, 2892−2926.

(34) Dobrawa, R.; Ballester, P. In *Metal-Containing and Metallo-supramolecular Polymers and Materials*; Schubert, U. S., Newkome, G. R., Eds.; ACS Symposium Series 928; American Chemical Society: Washington, DC, 2006; Vol. *4*, pp 43−62.

(35) Friese, V. A.; Kurth, D. G. *Curr. Opin. Colloid Interface Sci.* **2009**, *14*, 81−93.

(36) Haensch, C.; Chiper, M.; Ulbricht, C.; Winter, A.; Hoeppener, S.; Schubert, U. S. *Langmuir* **2008**, *24*, 12981−12985.
(37) Tarlov, M. J.; Burgess, D. R. F., Jr.; Gillen, G. *J. Am. Chem. Soc.* **1993**, *115*, 5305−5306.
(38) Xia, Y.; Whitesides, G. M. *Annu. Rev. Mater. Sci.* **1998**, *28*, 153−184.
(39) Salaita, K.; Wang, Y.; Mirkin, C. D. *Nat. Nanotechnol.* **2007**, *2*, 145−155.
(40) Georgakilas, V.; Otyepka, M.; Bourlinos, A. B.; Chandra, V.; Kim, N.; Kemp, K. C.; Hobza, P.; Zboril, R.; Kim, K. S. *Chem. Rev.* **2012**, *112*, 6156−6214.
(41) Holyer, R. H.; Hubbard, C. D.; Kettle, S. F. A.; Wilkins, R. G. *Inorg. Chem.* **1966**, *5*, 622−625.
(42) Jensen, P. W.; Jørgensen, L. B. *J. Mol. Struct.* **1982**, *79*, 87−92.
(43) Hansen, W.; Jensen, P. W. *Spectrochim. Acta* **1994**, *50*, 169−183.
(44) Coe, B. J.; Thompson, D. W.; Culbertson, C. T.; Schoonover, J. R.; Meyer, T. J. *Inorg. Chem.* **1995**, *34*, 3385−3395.
(45) Presselt, M.; Dietzek, B.; Schmitt, M.; Popp, J.; Winter, A.; Chiper, M.; Friebe, C.; Schubert, U. S. *J. Phys. Chem. C* **2008**, *112*, 18651−18668.
(46) Heinze, K.; Hempel, K.; Tschierlei, S.; Schmitt, M.; Popp, J.; Rau, S. *Eur. J. Inorg. Chem.* **2009**, *21*, 3119−3126.
(47) Winter, A. *ChemPhysChem* **2009**, *10*, 787−798.
(48) Siebert, R.; Schlütter, F.; Winter, A.; Presselt, M.; Göris, H.; Schubert, U. S.; Dietzek, B.; Popp, J. *Cent. Eur. J. Chem.* **2011**, *9*, 990−999.
(49) Myers, A. B. *Chem. Rev.* **1996**, *96*, 911−926.
(50) Zheng, Z.; Nottbohm, C. T.; Turchanin, A.; Muzik, H.; Beyer, A.; Heilemann, M.; Sauer, M.; Gölzhäuser, A. *Angew. Chem., Int. Ed.* **2010**, *49*, 8493−8497.
(51) Winter, A.; Friebe, C.; Hager, M. D.; Schuber, S. *Eur. J. Org. Chem.* **2009**, *6*, 801−809.
(52) VandeVondele, J.; Krack, M.; Mohamed, F.; Parrinello, M.; Chassaing, T.; Hutter, J. *Comput. Phys. Commun.* **2005**, *167*, 103−128.
(53) The CP2K developers group; http://www.cp2k.org/, 2014.
(54) Hasenknopf, B.; Lehn, J.-M.; Boumediene, N.; Dupont-Gervais, A.; Van Dorsselaer, A.; Kneisel, B.; Fensker, D. *J. Am. Chem. Soc.* **1997**, *119*, 10956−10962.
(55) Lee, C.; Wei, X.; Kysar, J. W.; Hone, J. *Science* **2008**, *321*, 385−388.
(56) Tang, W.; Thorpe, M. F. *Phys. Rev. B* **1988**, *37*, 5539−5551.
(57) Kudin, K. N.; Scuseria, G. E. *Phys. Rev. B* **2001**, *64*, 235406.
(58) Ostoja-Starzewski, M. *Appl. Mech. Rev.* **2002**, *55*, 35−60.
(59) Hogg, R.; Wilkins, R. G. *J. Chem. Soc.* **1962**, 341−350.